
ThermoHands: A Benchmark for 3D Hand Pose Estimation from Egocentric Thermal Images

Fangqiang Ding^{1,*} Yunzhou Zhu^{1,*} Xiangyu Wen¹ Gaowen Liu² Chris Xiaoxuan Lu^{3,†}
¹University of Edinburgh ²Cisco ³UCL

Abstract

In this work, we present ThermoHands, a new benchmark for thermal image-based egocentric 3D hand pose estimation, aimed at overcoming challenges like varying lighting conditions and obstructions (e.g., handwear). The benchmark includes a multi-view and multi-spectral dataset collected from 28 subjects performing hand-object and hand-virtual interactions under diverse scenarios, accurately annotated with 3D hand poses through an automated process. We introduce a new baseline method, TherFormer, utilizing dual transformer modules for effective egocentric 3D hand pose estimation in thermal imagery. Our experimental results highlight TherFormer’s leading performance and affirm thermal imaging’s effectiveness in enabling robust 3D hand pose estimation in adverse conditions.

1 Introduction

Egocentric 3D hand pose estimation is critically important for interpreting hand gestures across various applications, ranging from extended reality (XR) [1–4], to human-robot interaction [5–7], and to imitation learning [8–10]. Its importance has been magnified with the advent of advanced XR headsets such as the Meta Quest series [11] and Apple Vision Pro [12], where it serves as a cornerstone for spatial interaction and immersive digital experiences.

While current research of hand pose estimation primarily focuses on RGB image-based methods [13–17], these approaches are particularly vulnerable to issues related to lighting variation and occlusions caused by handwear, e.g., gloves or large jewellery [18, 19]. These challenges underscore the imperative for robust egocentric 3D hand pose estimation capable of performing reliably in a variety of common yet complex daily scenarios. The prevailing approach to facilitate robust hand pose estimation in low-light conditions utilizes *near infrared* (NIR) cameras paired with active NIR emitters. This technology, invisible to the human eye, leverages active NIR emitter-receiver configurations for depth estimation through time-of-flight (ToF) or structured lighting. Nevertheless, active NIR systems are more power-intensive compared to passive sensing technologies [20, 21] and are prone to interference from external NIR sources, such as sunlight [22] and other NIR-equipped devices [23]. Consequently, these vulnerabilities restrict the effectiveness of hand pose estimation under bright daylight conditions and in situations where multiple augmented reality (AR) or virtual reality (VR) systems are used for collaborative works.

In contrast to NIR-based methods, thermal imaging cameras offer a passive sensing solution for hand pose estimation by capturing long-wave infrared (LWIR) radiation emitted from objects, thereby eliminating reliance on the visible light spectrum [24]. This unique attribute of thermal imaging introduces several benefits for hand pose estimation. Primarily, it accentuates the hand’s structure via temperature differentials, negating the effects of lighting variability. Moreover, thermal cameras can detect hands even under handwear such as gloves by identifying heat transmission patterns. This

*Equal contribution

†Corresponding author: xiaoxuan.lu@ucl.ac.uk

ability ensures a stable and consistent representation of hands, independent of any coverings, thereby broadening the scope and reliability of hand pose estimation across various scenarios.

Building on the above insights, this study probes the following research question: *Can egocentric thermal imagery be effectively used for 3D hand pose estimation under various conditions (such as different lighting and handwear), and how does it compare to techniques using RGB, NIR, and depth³ spectral imagery?* To answer this, we introduce ThermoHands, the first benchmark specifically tailored for egocentric 3D hand pose estimation utilizing thermal imaging. This benchmark is supported by a novel multi-spectral and multi-view dataset designed for egocentric 3D hand pose estimation and is unique in comprising thermal, NIR, depth, and RGB images (cf. Fig. 1). Our dataset emulates real-world application contexts by incorporating both hand-object and hand-virtual interaction activities, with participation from 28 subjects to ensure a broad representation of actions. To offer a thorough comparison across spectral types, we gather data under five distinct scenarios, each characterized by varying environments, handwear, and lighting conditions (cf. Tab. 1). Considering the challenges associated with manually annotating large-scale 3D hand poses, we developed an automated annotation pipeline. This pipeline leverages multi-view RGB and depth imagery to accurately and efficiently generate 3D hand pose ground truths through optimization based on the MANO model [25] (cf. Fig. 3).

Together with the multi-spectral dataset, we introduce a new baseline method named *TherFormer*, specifically designed for thermal image-based egocentric 3D hand pose estimation (cf. Fig. 4). This approach is notable for its two consecutive transformer modules, *i.e.*, mask-guided spatial transformer and temporal transformer, which encode spatio-temporal relationship for 3D hand joints without losing the computation efficiency. Our validation process begins with verifying the annotation quality, which averages an accuracy of 1cm (cf. Tab. 2). We then benchmark *TherFormer* against leading methods (cf. Tab. 3) and compare the performance of various spectral images (cf. Tab. 4 and Fig. 6). The findings underscore thermal imagery’s advantages in difficult lighting conditions and when hands are gloved, showing superior performance and better adaptability to challenging settings than other spectral techniques. Our main contributions are summarized as follows:

- We introduce the first-of-its-kind benchmark, dubbed ThermoHands, to investigate the potential of thermal imaging for egocentric 3D hand pose estimation.
- We collected a diverse dataset comprising approximately 96,000 synchronized multi-spectral, multi-view images capturing hand-object and hand-virtual interactions from 28 participants across various environments. This dataset is enriched with 3D hand pose ground truths through an innovative automatic annotation process.
- We introduce a new baseline method, termed *TherFormer*, and implement state-of-the-art image-based methods on our dataset for benchmarking.
- Based on the ThermoHands benchmark, we conduct comprehensive experiments and analysis on TherFormer and state-of-the-art methods.
- We will release our dataset, code and models and maintain the benchmark to serve as a new challenge in 3D hand pose estimation.

2 Related Works

2.1 3D Hand Pose Datasets

Datasets with 3D hand pose annotations are imperative for training and evaluating *ad-hoc* models. Existing datasets, according to their approaches of annotation acquisition, can be summarized as four types in general, *i.e.*, marker-based [26–29], synthetic [30–34], manual [30, 35] or hybrid [36–40], and automatic [41–44] annotated datasets. Marker-based approaches, using magnetic sensor [26, 27] or Mocap markers [28, 29], can alter and induce bias to the hand appearance. Synthetic data [30–34] suffers from the *sim2real* gap in terms of hand motion and texture features. Introducing human annotators to fully [30, 35] or partly [36–40] annotate 2D/3D keypoints circumvents the issues above, but it either limits the scale of datasets or manifests costly and laborious in practice. Most similar to ours, some datasets adopt fully automatic pipelines to obtain 3D hand pose annotations [41–43], which leverage pre-trained models (*e.g.* OpenPose [45]) to infer the prior hand information and rely on optimization to fit the MANO hand model [25].

³For readability, we treat depth and NIR as two ‘spectra’, despite their usual overlap.

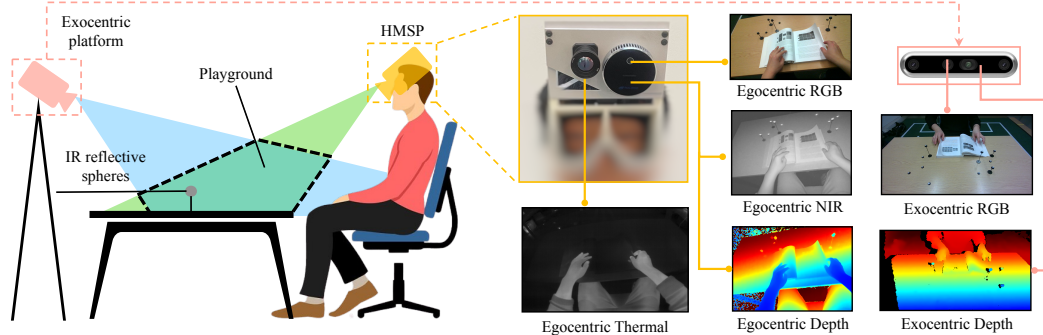


Figure 1: **Data capture setup** with the HMSP and exocentric platform recording multi-view multi-spectral images of two-hand actions performed by participants.

Despite the existing progress, previous datasets only provide depth [26, 32], RGB images [33, 37, 38, 40] or both of them [27, 28, 30, 31, 34–36, 39, 41–43] as the input spectra, unable to support the study of NIR or thermal image-based 3D hand pose estimation. ThermoHands fills the gap by providing a moderate amount of multi-spectral image data, from infrared to visual light, paired with depth images. Moreover, we capture bimanual actions from both egocentric and exocentric viewpoints and design hand-object as well as hand-virtual interaction actions to facilitate a wide range of applications.

2.2 Image-based 3D Hand Pose Estimation

As a key computer vision task, 3D hand pose estimation from images is highly demanded by applications like XR [1–4], human-robot interaction [5–7] and imitation learning [8–10]. Therefore, this field has been extensively explored in previous arts that uses single RGB [13, 14, 31, 38, 46–57] or depth [58–62] image as input. These methods can be roughly categorized into two fashions, *i.e.*, model-based and model-free methods. Model-based methods [14, 31, 51–57] utilize the prior knowledge of the MANO hand model [25] by estimating its shape and pose parameters, while model-free methods [13, 38, 46–50, 58–62] learn the direct regression of 3D hand joints or vertices coordinates. Recently there has been growing interest in leveraging the temporal supervision [54, 63–66] or leveraging sequential images as input [15–17, 67–69] for 3D hand pose estimation. In this study, we evaluate existing methods and our baseline method in both single image-based and video-based problem settings, respectively. Apart from the previous approaches, we investigate the potential of thermal imagery for tackling various challenges in 3D hand pose estimation.

2.3 Thermal Computer Vision

Thermal cameras achieve imaging by capturing the radiation emitted in the LWIR spectrum and deducing the temperature distribution on the surfaces [24]. Leveraging its robustness to variable illumination and unique temperature information, numerous efforts have been made to address various computer vision tasks, including super-resolution [70–72], human detection [73–75], action recognition [76, 77] and pose estimation [78–80], semantic segmentation [81–84], depth estimation [85–88], visual(-inertial) odometry/SLAM [89–92], 3D reconstruction [93–95], *etc.* In this work, we focus on 3D hand pose estimation, which is an under-exploited task based on thermal images.

3 The ThermoHands Benchmark

3.1 Multi-Spectral Hand Pose Dataset

Overview. At the core of our benchmark lies a multi-spectral dataset for 3D hand pose estimation (*cf.* Tab. 1), capturing hand actions performed by 28 subjects of various ethnicities and genders⁴. As shown in Fig. 1, we develop a customized head-mounted sensor platform (HMSP) and an exocentric platform to record multi-view data. During the capture, our participants are asked to perform pre-defined hand-object and hand-virtual interaction actions within the playground above the table. The

⁴The study has received the ethical approval from School of Informatics, University of Edinburgh, and participant consent forms were signed before the collection.

Setting	Normal office (Main)				Other settings				Total
	train	val	test	sum	darkness	sun glare	gloves	kitchen	
#frames	47,436	12,914	24,002	84,352	3,188	2,508	3,068	2,808	95,924
#seqs	172	43	86	301	12	12	12	14	352
#subjects	16	4	8	28	1	1	1	2	-

Table 1: **Benchmark Dataset Statistics.** The overall duration of our dataset is over 3 hours with $\sim 96K$ synchronized frame of all types of images collected.

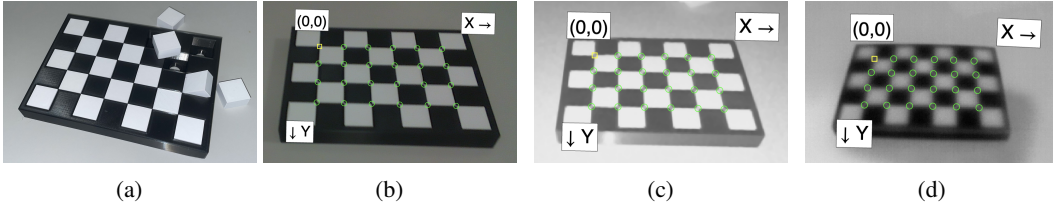


Figure 2: **Thermal calibration chessboard** containing a black base board and multiple removable white cubes (a). By cooling down the base board, it shows similar patterns and allows automatic corner detection in all (b) RGB, (c) NIR and (d) thermal images.

main part is captured in the normal office scenario. To facilitate the evaluation under different settings, four auxiliary parts are recorded i) under the darkness, ii) under the sun glare, iii) with gloves on hand, and iv) in the kitchen environment with different actions, respectively.

Sensor Platforms. The HMSP is mounted with an Intel RealSense L515 LiDAR depth camera [20] streaming egocentric RGB, depth and NIR images, and a FLIR Boson 640 thermal camera [96] receiving the LWIR to obtain the thermal images. To better simulate XR devices, the HMSP is modularly designed as two components: a base and a sensor board with a fixed 30-degree downward tilt. An extra exocentric platform equipped with an Intel RealSense D455 [21] is leveraged to support multi-view annotation (*cf.* Sec. 3.2) as well as provide the RGB-D image data from the third-person viewpoint. As exhibited in Fig. 1, we place the two depth sensors outside each other’s field of view (FoV) to minimize interference caused by their NIR emitters [20, 21]. In the office environment, random heat sources, *e.g.*, servers and chargers, are strategically placed in the background to increase realism and introduce challenging factors into thermal images.

Synchronization. We use a single PC to simultaneously gather data streams from two sensor platforms, ensuring the synchronization of their timestamps. After collection, we synchronize six types of images, each with distinct frame rates, w.r.t. the timestamps of thermal images (8.5fps), thereby generating well-aligned multi-spectral, multi-view data samples as our released data.

Calibration. For accuracy, we use factory-calibrated intrinsic parameters from the D455 and L515 cameras [20, 21]. To better calibrate the parameters of the thermal camera, we self-design a modular calibration chessboard as shown in Fig. 2. Before calibration, we cool down the black base board while keeping the white cubes at room temperature to create a visible chessboard pattern in all three spectra, which can be seen in Fig. 2. In this way, we can simultaneously calibrate the intrinsic parameter of the L515 thermal camera and its extrinsic parameter w.r.t. the D455 RGB-D camera. To enable the calibration between the two viewpoints, we place 11 IR reflective spheres at random locations and heights above the table. At the first frame of each sequence, we manually annotate their 2D locations from two viewpoints, retrieve their depth values and compute the transformation between two viewpoints by solving the PnP problem [97]. For the subsequent frames, as the exocentric platform keeps stationary, we only track the motion of the ego-head using KISS-ICP [98] odometry method, which takes the point clouds converted from the egocentric depth image as input.

Dataset Statistics. As seen in Tab. 1, our dataset consists of approximately 96K synchronized multi-spectral multi-view frames (*cf.* Fig. 1) and 352 independent sequences in total. The main part is collected under the normal office scenario, where each participant⁵ performs 7 hand-object interaction actions: *cut paper*, *fold paper*, *pour water*, *read book*, *staple paper*, *write with pen*, *write with pencil*, and 5 hand-virtual interaction actions: *pinch and drag*, *pinch and hold*, *swipe*, *tap*, *touch*, with two hands. This main part is divided into the training, validation and testing splits by subjects

⁵Due to their limited time, 7 participants only perform the hand-object actions.

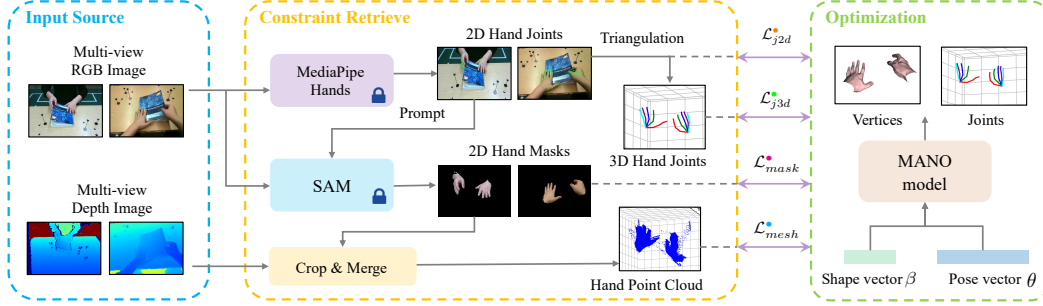


Figure 3: **Automatic annotation pipeline** of 3D hand pose. We utilize the multi-view RGB and depth images as the input source and retrieve constraint information with off-the-shelf MediaPipe Hands [99] and SAM [100]. Various error terms are formulated to optimize the MANO parameters.

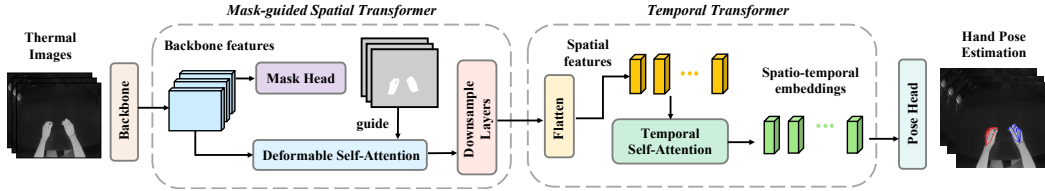


Figure 4: **Overall Framework of TherFormer**. Backbone features are input to the mask-guided spatial transformer and temporal transformer to enhance the spatial representation and temporal interaction. Spatio-temporal embeddings are fed into the pose head to regress the 3D hand pose.

with a ratio of 4:1:2. We also collect four auxiliary testing sets by asking one subject to perform the aforementioned 12 actions in the darkness, sun glare and gloves settings individually, and two subjects to perform 7 scenarios-specific interaction actions: *cut*, *spray*, *stir*, *wash hands*, *wash mug*, *wash plate*, *wipe* in the kitchen. Please refer to the supplementary for more dataset details.

3.2 Hand Pose Annotation

To avoid employing tedious human efforts for annotation, we implement a fully automatic annotation pipeline, similar to the approaches in [41–43], to obtain the 3D hand pose ground truth for our dataset. In particular, we use the MANO statistical hand model [25] to represent 3D hand pose. The MANO model parameterizes the hand mesh vertices into two low-dimensional embeddings, *i.e.*, the shape parameters $\beta \in \mathbb{R}^{10}$ and the pose parameters $\theta \in \mathbb{R}^{51}$. The MANO fitting is performed by minimizing the following optimization objective per frame for each hand:

$$\theta^* = \arg \min_{\theta} \lambda_{j2d} \mathcal{L}_{j2d}^{\bullet} + \lambda_{mask} \mathcal{L}_{mask}^{\bullet} + \lambda_{j3d} \mathcal{L}_{j3d}^{\bullet} + \lambda_{mesh} \mathcal{L}_{mesh}^{\bullet} + \lambda_{reg} \mathcal{L}_{reg}^{\bullet} \quad (1)$$

where λ_{j2d} , λ_{mask} , λ_{j3d} , λ_{mesh} , λ_{reg} are used to balance the weight of different errors. The diagram illustrating our annotation process is shown in Fig. 3. For more explanation of error terms and implementation details of our dataset annotation process, please refer to our supplementary document.

3.3 TherFormer: A Baseline Method

For our benchmark, we setup a baseline method, dubbed TherFormer, for thermal image-based 3D hand pose estimation. As exhibited in Fig. 4, TherFormer features in its two consecutive transformer modules to model the spatio-temporal relationship of hand joints while being computationally efficient. Note that TherFormer is also capable of processing other spectral images due to their format consistency with thermal images. However, our primary objective is to establish a baseline method for future research, rather than focusing exclusively on methods for thermal images.

Problem Definition. We consider two problem settings: single image-based and video-based egocentric 3D hand pose estimation for our benchmark. In the former setting, we aim to estimate the 3D joint positions \mathcal{J}_t for two hands given the single thermal image \mathcal{I}_t captured for the t -th frame. For the video-based one, our input is a sequence of thermal images $\mathcal{S} = \{\mathcal{I}_i\}_{i=1}^T$ and we estimate the per-frame 3D hand joint positions \mathcal{J}_i together. Without losing the generality, here we illustrate our

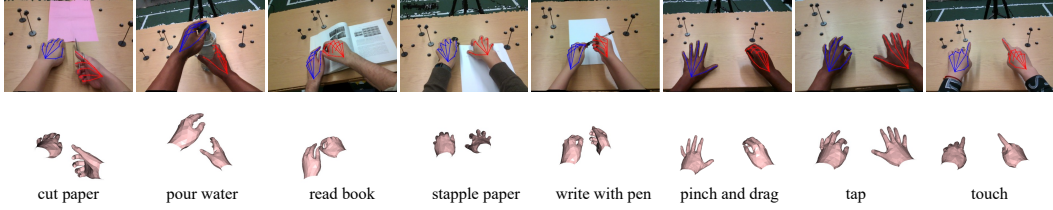


Figure 5: Examples of 3D hand pose annotations. Top row: left (blue) and right (red) hand 3D joints projected onto egocentric RGB images. Bottom row: visualization of hand mesh annotation.

network architecture for the video-based setting, *i.e.*, TherFormer-V. In practice, our network can be flexibly adapted to the single image-based version (*i.e.*, TherFormer-S) by setting $T = 1$.

Mask-guided Spatial Transformer. Human hands are highly articulated objects that can adopt a wide variety of poses, often against complex backgrounds. We propose a mask-guided spatial transformer module to accurately identify and focus on the intricacies of hand poses during spatial feature interaction. Given backbone features, we first utilize a mask head to estimate the binary hand mask in the thermal image. Then, we leverage the deformable self-attention [101] to refine the hand spatial features under the guidance of the estimated hand mask. Specifically, we only take feature elements whose spatial locations are within the hand area as queries and sample keys from only the hand area and its surrounding locations. In this way, we not only reduce the computation waste on the irrelevant region but also increase the robustness to background clutter. Lastly, we reduce the spatial dimensions of the spatial features with a series of convolutions layers for efficiency.

Temporal Transformer. Temporal information is crucial for 3D hand pose estimation when coping with occlusion and solving ambiguities. To model temporal relationships, we first flatten the spatial features into 1D feature vectors and then employed the temporal self-attention [102] to explicitly attend to the feature vector of every frame. The output is frame-wise spatio-temporal feature embeddings. Note that the temporal self-attention degrades to an MLP for single-image based setting.

In the pose head, we use the MLP to project the embeddings to the output space and obtain the per-frame 3D joint \mathcal{J}_i . We leverage the binary cross-entropy loss to supervise the hand segmentation with the mask ground truth rendered from the annotated hand mesh (*cf.* Sec. 3.2). For 3D hand joint positions, we measure the $L1$ distance of its 2D projection and depth to that of the ground truth separately. Please see more details of TherFormer in our supplementary document.

4 Experiment

4.1 Evaluation of the Annotation Method

As the first step, we validate the accuracy of our 3D hand pose annotation (*cf.* Sec. 3.2) and analyze the impact for optimization results. For evaluation, we manually annotate two random sequences from our main dataset, with a total of over 600 frames. To that end, we first annotate the 2D joint locations from both egocentric and exocentric images and obtain the 3D joint positions by triangulation. We calculate the average 3D joint errors across all frames to measure the accuracy.

As shown in Tab. 2, our annotation method achieves an average joint error of nearly 1cm, comparable to the results of [37, 41, 43]. The multi-view setting shows remarkably better precision than the ego-view only optimization, demonstrating the necessity of multi-camera capture. We also observe that only combining \mathcal{L}_{mask} and \mathcal{L}_{j2d} can already provide a plausible accuracy since they fit the projection of the 3D hand pose to two heterogeneous views. \mathcal{L}_{mesh} , though it hardly improves the joint accuracy, can result in more natural hand mesh. Adding \mathcal{L}_{j3d} further refines the joints as it induces the explicit constraint to their positions. We showcase some annotation examples in Fig. 5. As can be seen, both hand joint and mesh can be accurately annotated across different actions despite the presence of occlusion and the variance in subjects’ hand color and shape.

4.2 Experiment Setup

Dataset Preparation. We utilize our own dataset for experiments as it uniquely contains egocentric images from multiple spectra, essentially for our benchmark experiments. We annotate the main part

Errors	Ego-view optimization			Multi-view optimization		
	$\mathcal{L}_{mask} + \mathcal{L}_{j2d}$	$\mathcal{L}_{mask} + \mathcal{L}_{j2d} + \mathcal{L}_{mesh}$	\mathcal{L}_{mask}	$\mathcal{L}_{mask} + \mathcal{L}_{j2d}$	$\mathcal{L}_{mask} + \mathcal{L}_{j2d} + \mathcal{L}_{mesh}$	$\mathcal{L}_{mask} + \mathcal{L}_{j2d} + \mathcal{L}_{mesh} + \mathcal{L}_{j3d}$
mean (std)	37.29 (\pm 18.02)	7.03 (\pm 2.57)	8.13 (\pm 0.57)	1.29 (\pm 0.43)	1.28 (\pm 0.43)	1.01 (\pm 0.34)

Table 2: Evaluation of annotation results. The average 3D joint errors across all frames are reported (in cm). \mathcal{L}_{reg} is used for all to mitigate irregular hand poses.

	Method	Input	MEPE (mm) ↓	AUC ↑	MEPE-RA (mm) ↓	AUC-RA ↑	fps ↑
(a)	A2J-Transformer [46]	Single	51.68	0.474	20.76	0.603	34
(b)	HTT [15]	Single	49.09	0.489	20.69	0.599	211
(c)	TherFormer-S	Single	44.64	0.539	18.34	0.643	136
(d)	(c) w/o spatial transformer	Single	48.79	0.491	20.15	0.609	174
(e)	(c) w/o mask guidance	Single	48.83	0.494	18.89	0.625	141
(f)	HTT [15]	Sequence	47.07	0.512	17.49	0.659	129
(g)	TherFormer-V	Sequence	43.36	0.549	17.36	0.661	52

Table 3: Comparison between TherFormer and state of the arts on thermal camera-based 3D hand pose estimation. The fps indicates the number of inference steps that models can run per second.

of our dataset (*cf.* Tab. 1) automatically following Sec. 3.2, of which the training and validation sets serve as the foundation for the training of all network models.

Method and Implementation. To provide sufficient baselines for follow-up works, we selected two state-of-the-art methods in 3D hand pose estimation: HTT [15] and A2J-Transformer [46], and reproduced them on our dataset for experiments. HTT [15] is a video-based method thus enabling the evaluation in both two problem settings while A2J-Transformer [46] only works under the single image-based setting. For a feasible comparison, we use the same sequence length, *i.e.*, $T = 8$, for HTT and TherFormer-V baselines. We exclude the additional action block used by HTT [15], focusing solely on hand pose estimation. We adjusted the anchor initialization phase of A2J-Transformer [46] to better accommodate our dataset, without altering the density of its anchors. All trained models are tested on a single NVIDIA RTX 4090 GPU to fairly compare their inference speed.

Evaluation Metrics. We evaluate the accuracy of 3D hand pose estimation with two metrics: *Percentage of Correct Keypoints* (PCK) and *Mean End-Point Error* (MEPE) [34], in both camera space and root-aligned (RA) space [38]. For RA space, we align the estimated wrist with its groundtruth position before measurement. For PCK, we report the corresponding *Area Under the Curve* (AUC) over the 0-50mm/80mm error thresholds for the camera/RA space.

4.3 Thermal Image-based 3D Hand Pose Estimation

Main Results. To assess TherFormer’s performance in thermal image-based 3D hand pose estimation, we compare it against state-of-the-art methods [15, 46] on the main testing set, as shown in Tab. 3. TherFormer-S outforms two competing methods under the single image-based setting, while TherFormer-V surpasses the counterpart HTT [15] given the same sequential images as input. Such an improvement mainly stems from our mask-guided spatial attention design that can adaptively encode the spatial interaction among hand joints with the guidance of the hand mask (*cf.* Sec. 3.3). A performance gap can be observed between single image-based and video-based settings for both HTT [15] and TherFormer. We credit this to their usage of temporal information that helps to tackle the occlusion cases and solve ambiguities. Thanks to our lightweight network design, TherFormer is highly efficient to run with fps of 136 and 52 for single and sequence input respectively, ensuring its real-time application to resource-constrained devices. Moreover, TherFormer-V also improves the performance over HTT [15] for other spectra (*cf.* Tab. 4), proving its adaptability to different inputs.

Ablation Studies. We ablate our proposed mask-guided attention mechanism and the entire spatial transformer (*cf.* Sec. 3.3) to observe their impact. As can be seen in Tab. 3, the mask-guided attention mechanism notably contributes to TherFormer’s performance growth (row (c) vs. (e)), demonstrating its effectiveness in mitigating the effect of background clutter. Other components in the spatial transformer bring a large performance gain in the RA space (row (e) vs. (d)), confirming the importance of spatial feature enhancement for fine-grained hand joints localization.

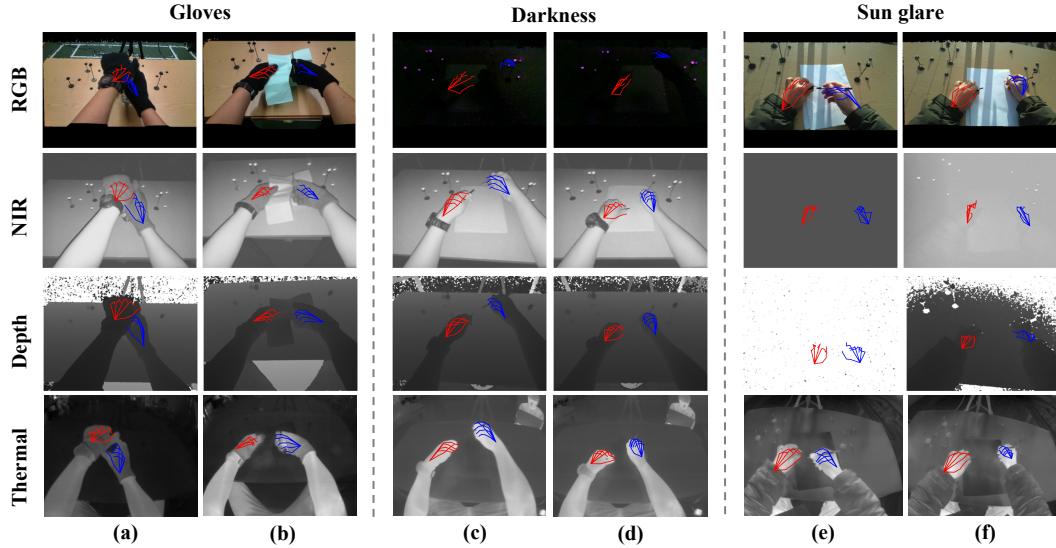


Figure 6: Examples of results with various spectra under three challenging settings. For visualization, we show the projection of the estimated left (red) and right (blue) 3D hand joints on images.

4.4 Comparison between Spectrum

4.4.1 Qualitative Results under Challenging Conditions

To justify the advantages of using thermal cameras for egocentric hand pose estimation under challenging scenarios, we conduct a comparison between four spectra on three of our auxiliary testing sets, *i.e.*, gloves, darkness and sun glare (*cf.* Tab. 1). Our automatic annotation pipeline (*cf.* Sec. 3.2) becomes infeasible since hands appear corrupted in either RGB or depth images. Therefore, we conduct a qualitative analysis of their performance and present some representative examples in Fig. 6. We use the same model, *i.e.*, HTT [15], trained on different spectra for a fair comparison. Please see the supplementary materials for more figure examples and demo videos under challenging conditions.

RGB vs. Thermal. As can be seen, RGB-based methods fail with gloves wearing (*cf.* Fig. 6 (a-b)) and in darkness (*cf.* Fig. 6 (c-d)). Gloves change how human hands look and hide their natural colors and textures. Since RGB algorithms rely on skin’s texture and color to identify hand parts and joints, gloves, particularly those with solid colors or textures unlike skin, can interfere with this identification process. Contrary to RGB techniques, as shown in Fig. 6 (a-b), thermal imaging methods excel in identifying hands by leveraging the principles of heat conduction through gloves, effectively bypassing the limitations imposed by color and texture variations.

NIR, Depth vs. Thermal. NIR sensors are significantly disrupted by strong sunlight, affecting both NIR imaging and depth map creation, as shown in Fig. 6 (e-f). Conversely, thermal imaging is immune to sunlight and outdoor conditions. The temperature difference between hands and their surroundings in the thermal spectrum facilitates effortless identification of the hands, leaving the thermal-based estimator unaffected. The thermal camera’s ability to consistently capture hand features in diverse lighting conditions positions it as a suitable option for future XR applications.

4.4.2 Quantitative Results under Normal Conditions

To validate the versatility of thermal-based methods, we also evaluate their performance compared to other spectra (*i.e.*, RGB, depth, NIR and thermal) under normal conditions for general-purpose use cases. We apply different spectral images as input to multiple baselines methods and report the results in Tab. 4. Not surprisingly, depth image-based methods yield the best performance on average, as they directly utilize the depth information to provide a detailed 3D structure of the hand. The NIR spectrum shows a marginal decrease in performance compared to depth but outperforms both RGB and thermal spectra. This can be attributed to NIR camera’s active sensing ability, which leads to more consistent and reliable imaging regardless of the variability of external illuminations (*vs.* RGB) and temperature (*vs.* thermal). However, active NIR sensors are prone to interference from external NIR

Spectrum	HTT (Sequence)		TherFormer-V		TherFormer-S		Average	
	MEPE (mm) ↓	AUC ↑	MEPE (mm) ↓	AUC ↑	MEPE (mm) ↓	AUC ↑	MEPE (mm) ↓	AUC ↑
RGB	43.30	0.542	43.50	0.542	44.61	0.529	43.80	0.538
Depth	41.62	0.559	39.70	0.581	39.84	0.579	40.39	0.573
NIR	41.57	0.562	40.79	0.575	40.98	0.575	41.11	0.571
Thermal	47.07	0.512	43.36	0.549	44.64	0.539	45.06	0.533

Table 4: Comparison between different spectra under normal conditions. Models are trained with their corresponding spectrum images from the training set. We test them on the main testing set.

sources like sun glare (*cf.* Fig. 6). Thermal-based methods, despite using single-channel heat capture, achieves comparable performance to those using RGB images that contain rich color and textures. Such results suggest that thermal images can not only serve as supplements in challenging cases but also can be a viable alternative to other spectra in normal conditions for hand pose estimation.

5 Limitation and Future Work

Despite the advancements, we acknowledge certain limitations here guiding our future work. First, the scale of our current dataset is relatively small when compared to some datasets [29, 38–40]. We plan to continuously enlarge this dataset by incorporating data from new scenarios and hand actions. Second, we only annotate 3D hand pose for our dataset, which limits its usage of evaluation to other tasks relevant to human hands. Further efforts will be annotating the fine-grained hand action splits and contact heatmap for hand grasp [42]. Lastly, we currently rely on qualitative analysis for challenging conditions when our automatic annotation method becomes unreliable. In the future, we will leverage unaffected spectral images in individual cases to manually annotate the 3D hand pose.

6 Conclusion

This paper introduces ThermoHands, the first benchmark for egocentric 3D hand pose estimation using thermal images. It features a multi-spectral, multi-view dataset with automatically annotated 3D poses and a novel baseline method utilizing dual transformer modules for encoding spatio-temporal relationships. We demonstrate near 1cm annotation accuracy, show that TherFormer surpasses existing methods in thermal-based 3D hand pose estimation, and confirm thermal images’ effectiveness in challenging lighting and obstruction scenarios. We believe our endeavour could pave the way for further research in thermal-based 3D hand pose estimation and its wide application.

Acknowledgments and Disclosure of Funding

This research is partially supported by the Engineering and Physical Sciences Research Council (EPSRC) under the Centre for Doctoral Training in Robotics and Autonomous Systems at the Edinburgh Centre of Robotics (EP/S023208/1), and partially supported by Cisco Research.

References

- [1] Min-Yu Wu, Pai-Wen Ting, Ya-Hui Tang, En-Te Chou, and Li-Chen Fu. Hand pose estimation in object-interaction based on deep learning for virtual reality applications. *J. Vis. Commun. Image Represent.*, 70:102802, 2020. 1, 3
- [2] K Martin Sagayam and D Jude Hemanth. Hand posture and gesture recognition techniques for virtual reality applications: a survey. *Virtual Reality*, 21:91–107, 2017. 1, 3
- [3] Eric Marchand, Hideaki Uchiyama, and Fabien Spindler. Pose estimation for augmented reality: a hands-on survey. *TVCG*, 22(12):2633–2651, 2015. 1, 3
- [4] Hui Liang, Junsong Yuan, Daniel Thalmann, and Nadia Magnenat Thalmann. Ar in hand: Egocentric palm pose tracking and gesture recognition for augmented reality applications. In *ACM MM*, pages 743–744, 2015. 1, 3
- [5] Alessio Sampieri, Guido Maria D’Amely di Melendugno, Andrea Avogaro, Federico Cunico, Francesco Setti, Geri Skenderi, Marco Cristani, and Fabio Galasso. Pose forecasting in industrial human-robot collaboration. In *ECCV*, pages 51–69. Springer, 2022. 1, 3

- [6] Qing Gao, Yongquan Chen, Zhaojie Ju, and Yi Liang. Dynamic hand gesture recognition based on 3D hand pose estimation for human–robot interaction. *IEEE Sensors Journal*, 22(18):17421–17430, 2021. 1, 3
- [7] Qing Gao, Jinguo Liu, Zhaojie Ju, and Xin Zhang. Dual-hand detection for human–robot interaction by a parallel network based on hand detection and body pose estimation. *IEEE Transactions on Industrial Electronics*, 66(12):9663–9672, 2019. 1, 3
- [8] Yuzhe Qin, Yueh-Hua Wu, Shaowei Liu, Hanwen Jiang, Ruihan Yang, Yang Fu, and Xiaolong Wang. Dexmv: Imitation learning for dexterous manipulation from human videos. In *ECCV*, pages 570–587. Springer, 2022. 1, 3
- [9] Yuanpei Chen, Yiran Geng, Fangwei Zhong, Jiaming Ji, Jiechuang Jiang, Zongqing Lu, Hao Dong, and Yaodong Yang. Bi-DexHands: Towards Human-Level Bimanual Dexterous Manipulation. *PAMI*, 2023. 1, 3
- [10] Dafni Antotsiou, Guillermo Garcia-Hernando, and Tae-Kyun Kim. Task-oriented hand motion retargeting for dexterous manipulation imitation. In *ECCVW*, 2018. 1, 3
- [11] Meta. Meta Quest. <https://www.meta.com/gb/quest/>, 2024. Accessed: 2024-02-23. 1
- [12] Apple. Apple Vision Pro. <https://www.apple.com/apple-vision-pro/>, 2024. Accessed: 2024-02-23. 1
- [13] Fanqing Lin, Connor Wilhelm, and Tony Martinez. Two-hand global 3d pose estimation using monocular rgb. In *WACV*, pages 2373–2381, 2021. 1, 3
- [14] Mengcheng Li, Liang An, Hongwen Zhang, Lianpeng Wu, Feng Chen, Tao Yu, and Yebin Liu. Interacting attention graph for single image two-hand reconstruction. In *CVPR*, pages 2761–2770, 2022. 1, 3
- [15] Yilin Wen, Hao Pan, Lei Yang, Jia Pan, Taku Komura, and Wenping Wang. Hierarchical temporal transformer for 3d hand pose estimation and action recognition from egocentric rgb videos. In *CVPR*, pages 21243–21253, 2023. 1, 3, 7, 8, 15
- [16] Qichen Fu, Xingyu Liu, Ran Xu, Juan Carlos Niebles, and Kris M. Kitani. Deformer: Dynamic Fusion Transformer for Robust Hand Pose Estimation. In *ICCV*, pages 23600–23611, October 2023. 1, 3
- [17] Hoseong Cho, Chanwoo Kim, Jihyeon Kim, Seongyeong Lee, Elkhan Ismayilzada, and Seungryul Baek. Transformer-Based Unified Recognition of Two Hands Manipulating Objects. In *CVPR*, pages 4769–4778, 2023. 1, 3
- [18] Trenton’s Tech. Testing the Apple Vision Pro in Pitch Black Environments. YouTube, 2024. https://www.youtube.com/watch?v=w1Ppo_QFIRU. 1
- [19] Apple. Use gestures with Apple Vision Pro. <https://support.apple.com/en-us/117741>, 2024. Accessed: 2024-02-23. 1
- [20] Intel RealSense. LiDAR Camera L515. <https://www.intelrealsense.com/lidar-camera-l515/>, 2023. Accessed: 2024-02-27. 1, 4
- [21] Intel RealSense. Depth Camera D455. <https://www.intelrealsense.com/depth-camera-d455/>, 2023. Accessed: 2024-02-27. 1, 4
- [22] Jesus Suarez and Robin R Murphy. Using the kinect for search and rescue robotics. In *SSRR*, pages 1–2. IEEE, 2012. 1
- [23] Lucas Adams Seewald, Vinicius Facco Rodrigues, Malte Ollenschläger, Rodolfo Stoffel Antunes, Cristiano André da Costa, Rodrigo da Rosa Righi, Luiz Gonzaga da Silveira Jr, Andreas Maier, Björn Eskofier, and Rebecca Fahrig. Toward analyzing mutual interference on infrared-enabled depth cameras. *Computer Vision and Image Understanding*, 178:1–15, 2019. 1
- [24] J Michael Lloyd. *Thermal imaging systems*. Springer Science & Business Media, 2013. 1, 3
- [25] Javier Romero, Dimitrios Tzionas, and Michael J. Black. Embodied Hands: Modeling and Capturing Hands and Bodies Together. *TOG*, 36(6), 2017. 2, 3, 5
- [26] Shanxin Yuan, Qi Ye, Bjorn Stenger, Siddhant Jain, and Tae-Kyun Kim. Bighand2. 2m benchmark: Hand pose dataset and state of the art analysis. In *CVPR*, pages 4866–4874, 2017. 2, 3

- [27] Guillermo Garcia-Hernando, Shanxin Yuan, Seungryul Baek, and Tae-Kyun Kim. First-person hand action benchmark with rgb-d videos and 3d hand pose annotations. In *CVPR*, pages 409–419, 2018. [2](#), [3](#)
- [28] Omid Taheri, Nima Ghorbani, Michael J Black, and Dimitrios Tzionas. GRAB: A dataset of whole-body human grasping of objects. In *ECCV*, pages 581–600. Springer, 2020. [2](#), [3](#)
- [29] Zicong Fan, Omid Taheri, Dimitrios Tzionas, Muhammed Kocabas, Manuel Kaufmann, Michael J Black, and Otmar Hilliges. ARCTIC: A Dataset for Dexterous Bimanual Hand-Object Manipulation. In *CVPR*, pages 12943–12954, 2023. [2](#), [9](#)
- [30] Franziska Mueller, Dushyant Mehta, Oleksandr Sotnychenko, Srinath Sridhar, Dan Casas, and Christian Theobalt. Real-time hand tracking under occlusion from an egocentric rgb-d sensor. In *ICCV*, pages 1154–1163, 2017. [2](#), [3](#)
- [31] Yana Hasson, Gul Varol, Dimitrios Tzionas, Igor Kalevatykh, Michael J Black, Ivan Laptev, and Cordelia Schmid. Learning joint reconstruction of hands and manipulated objects. In *CVPR*, pages 11807–11816, 2019. [2](#), [3](#)
- [32] Franziska Mueller, Micah Davis, Florian Bernard, Oleksandr Sotnychenko, Mickeal Verschoor, Miguel A Otaduy, Dan Casas, and Christian Theobalt. Real-time pose and shape reconstruction of two interacting hands with a single depth camera. *TOG*, 38(4):1–13, 2019. [2](#), [3](#)
- [33] Franziska Mueller, Florian Bernard, Oleksandr Sotnychenko, Dushyant Mehta, Srinath Sridhar, Dan Casas, and Christian Theobalt. Generated hands for real-time 3d hand tracking from monocular rgb. In *CVPR*, pages 49–59, 2018. [2](#), [3](#)
- [34] Christian Zimmermann and Thomas Brox. Learning to estimate 3d hand pose from single rgb images. In *ICCV*, pages 4903–4911, 2017. [2](#), [3](#), [7](#)
- [35] Srinath Sridhar, Franziska Mueller, Michael Zollhöfer, Dan Casas, Antti Oulasvirta, and Christian Theobalt. Real-time joint tracking of a hand manipulating an object from rgb-d input. In *ECCV*, pages 294–310. Springer, 2016. [2](#), [3](#)
- [36] Yu-Wei Chao, Wei Yang, Yu Xiang, Pavlo Molchanov, Ankur Handa, Jonathan Tremblay, Yashraj S Narang, Karl Van Wyk, Umar Iqbal, Stan Birchfield, et al. DexYCB: A benchmark for capturing hand grasping of objects. In *CVPR*, pages 9044–9053, 2021. [2](#), [3](#)
- [37] Christian Zimmermann, Duygu Ceylan, Jimei Yang, Bryan Russell, Max Argus, and Thomas Brox. Freihand: A dataset for markerless capture of hand pose and shape from single rgb images. In *ICCV*, pages 813–822, 2019. [2](#), [3](#), [6](#)
- [38] Gyeongsik Moon, Shoou-I Yu, He Wen, Takaaki Shiratori, and Kyoung Mu Lee. Interhand2.6m: A dataset and baseline for 3d interacting hand pose estimation from a single rgb image. In *ECCV*, pages 548–564. Springer, 2020. [2](#), [3](#), [7](#), [9](#)
- [39] Yunze Liu, Yun Liu, Che Jiang, Kangbo Lyu, Weikang Wan, Hao Shen, Boqiang Liang, Zhoujie Fu, He Wang, and Li Yi. HOI4D: A 4D egocentric dataset for category-level human-object interaction. In *CVPR*, pages 21013–21022, 2022. [2](#), [3](#), [9](#)
- [40] Takehiko Ohkawa, Kun He, Fadime Sener, Tomas Hodan, Luan Tran, and Cem Keskin. AssemblyHands: Towards Egocentric Activity Understanding via 3D Hand Pose Estimation. In *CVPR*, pages 12999–13008, 2023. [2](#), [3](#), [9](#)
- [41] Shreyas Hampali, Mahdi Rad, Markus Oberweger, and Vincent Lepetit. Honnotate: A method for 3d annotation of hand and object poses. In *CVPR*, pages 3196–3206, 2020. [2](#), [3](#), [5](#), [6](#)
- [42] Samarth Brahmabhatt, Chengcheng Tang, Christopher D Twigg, Charles C Kemp, and James Hays. ContactPose: A dataset of grasps with object contact and hand pose. In *ECCV*, pages 361–378. Springer, 2020. [2](#), [3](#), [5](#), [9](#)
- [43] Taein Kwon, Bugra Tekin, Jan Stühmer, Federica Bogo, and Marc Pollefeys. H2o: Two hands manipulating objects for first person interaction recognition. In *ICCV*, pages 10138–10148, 2021. [2](#), [3](#), [5](#), [6](#)
- [44] Fadime Sener, Dibyadip Chatterjee, Daniel Sheleпов, Kun He, Dipika Singhanian, Robert Wang, and Angela Yao. Assembly101: A large-scale multi-view video dataset for understanding procedural activities. In *CVPR*, pages 21096–21106, 2022. [2](#)
- [45] Zhe Cao, Gines Hidalgo, Tomas Simon, Shih-En Wei, and Yaser Sheikh. OpenPose: Realtime Multi-Person 2D Pose Estimation Using Part Affinity Fields. *PAMI*, 43(1):172–186, 2021. [2](#)

- [46] Changlong Jiang, Yang Xiao, Cunlin Wu, Mingyang Zhang, Jinghong Zheng, Zhiguo Cao, and Joey Tianyi Zhou. A2J-Transformer: Anchor-to-Joint Transformer Network for 3D Interacting Hand Pose Estimation from a Single RGB Image. In *CVPR*, pages 8846–8855, 2023. 3, 7, 15
- [47] Adrian Spurr, Umar Iqbal, Pavlo Molchanov, Otmar Hilliges, and Jan Kautz. Weakly supervised 3d hand pose estimation via biomechanical constraints. In *ECCV*, pages 211–228. Springer, 2020. 3
- [48] Linlin Yang and Angela Yao. Disentangling latent hands for image synthesis and pose estimation. In *CVPR*, pages 9877–9886, 2019. 3
- [49] Wencan Cheng, Jae Hyun Park, and Jong Hwan Ko. Handfoldingnet: A 3d hand pose estimation network using multiscale-feature guided folding of a 2d hand skeleton. In *ICCV*, pages 11260–11269, 2021. 3
- [50] Dong Uk Kim, Kwang In Kim, and Seungryul Baek. End-to-end detection and pose estimation of two interacting hands. In *ICCV*, pages 11189–11198, 2021. 3
- [51] Breannan Smith, Chenglei Wu, He Wen, Patrick Peluse, Yaser Sheikh, Jessica K Hodgins, and Takaaki Shiratori. Constraining dense hand surface tracking with elasticity. *TOG*, 39(6):1–14, 2020. 3
- [52] Jiayi Wang, Franziska Mueller, Florian Bernard, Suzanne Sorli, Oleksandr Sotnychenko, Neng Qian, Miguel A Otaduy, Dan Casas, and Christian Theobalt. Rgb2hands: real-time tracking of 3d hand interactions from monocular rgb video. *TOG*, 39(6):1–16, 2020. 3
- [53] Baowen Zhang, Yangang Wang, Xiaoming Deng, Yinda Zhang, Ping Tan, Cuixia Ma, and Hongan Wang. Interacting two-hand 3d pose and shape reconstruction from single color image. In *ICCV*, pages 11354–11363, 2021. 3
- [54] Shaowei Liu, Hanwen Jiang, Jiarui Xu, Sifei Liu, and Xiaolong Wang. Semi-supervised 3d hand-object poses estimation with interactions in time. In *CVPR*, pages 14687–14697, 2021. 3
- [55] Adnane Boukhayma, Rodrigo de Bem, and Philip HS Torr. 3d hand shape and pose from images in the wild. In *CVPR*, pages 10843–10852, 2019. 3
- [56] Seungryul Baek, Kwang In Kim, and Tae-Kyun Kim. Pushing the envelope for rgb-based dense 3d hand pose estimation via neural rendering. In *CVPR*, pages 1067–1076, 2019. 3
- [57] Xiong Zhang, Qiang Li, Hong Mo, Wenbo Zhang, and Wen Zheng. End-to-end hand mesh recovery from a monocular rgb image. In *ICCV*, pages 2354–2364, 2019. 3
- [58] Liuhaohao Ge, Hui Liang, Junsong Yuan, and Daniel Thalmann. Robust 3D hand pose estimation from single depth images using multi-view CNNs. *IEEE Transactions on Image Processing*, 27(9):4422–4436, 2018. 3
- [59] Gyeongsik Moon, Ju Yong Chang, and Kyoung Mu Lee. V2v-posenet: Voxel-to-voxel prediction network for accurate 3d hand and human pose estimation from a single depth map. In *CVPR*, pages 5079–5088, 2018. 3
- [60] Fu Xiong, Boshen Zhang, Yang Xiao, Zhiguo Cao, Taidong Yu, Joey Tianyi Zhou, and Junsong Yuan. A2j: Anchor-to-joint regression network for 3d articulated pose estimation from a single depth image. In *Proceedings of the IEEE/CVF International Conference on Computer Vision*, pages 793–802, 2019. 3
- [61] Zhaohui Zhang, Shipeng Xie, Mingxiu Chen, and Haichao Zhu. HandAugment: A simple data augmentation method for depth-based 3D hand pose estimation. *arXiv preprint arXiv:2001.00702*, 2020. 3
- [62] Tianqiang Zhu, Yi Sun, Xiaohong Ma, and Xiangbo Lin. Hand Pose Ensemble Learning Based on Grouping Features of Hand Point Sets. In *ICCVW*, 2019. 3
- [63] Yana Hasson, Bugra Tekin, Federica Bogo, Ivan Laptev, Marc Pollefeys, and Cordelia Schmid. Leveraging photometric consistency over time for sparsely supervised hand-object reconstruction. In *CVPR*, pages 571–580, 2020. 3
- [64] John Yang, Hyung Jin Chang, Seungeui Lee, and Nojun Kwak. SeqHAND: RGB-sequence-based 3D hand pose and shape estimation. In *ECCV*, pages 122–139. Springer, 2020. 3
- [65] Muhammed Kocabas, Nikos Athanasiou, and Michael J. Black. VIBE: Video Inference for Human Body Pose and Shape Estimation. In *CVPR*, June 2020. 3

- [66] JoonKyu Park, Yeonguk Oh, Gyeongsik Moon, Hongsuk Choi, and Kyoung Mu Lee. Handocnet: Occlusion-robust 3d hand mesh estimation network. In *CVPR*, pages 1496–1505, 2022. 3
- [67] Yujun Cai, Lihao Ge, Jun Liu, Jianfei Cai, Tat-Jen Cham, Junsong Yuan, and Nadia Magnenat Thalmann. Exploiting Spatial-Temporal Relationships for 3D Pose Estimation via Graph Convolutional Networks. In *ICCV*, October 2019. 3
- [68] Leyla Khaleghi, Alireza Sepas-Moghaddam, Joshua Marshall, and Ali Etemad. Multi-view video-based 3D hand pose estimation. *IEEE Transactions on Artificial Intelligence*, 2022. 3
- [69] Hongsuk Choi, Gyeongsik Moon, Ju Yong Chang, and Kyoung Mu Lee. Beyond static features for temporally consistent 3d human pose and shape from a video. In *CVPR*, pages 1964–1973, 2021. 3
- [70] Rafael E Rivadeneira, Angel D Sappa, Boris X Vintimilla, Dai Bin, Li Ruodi, Li Shengye, Zhiwei Zhong, Xianming Liu, Junjun Jiang, and Chenyang Wang. Thermal Image Super-Resolution Challenge Results-PBVS 2023. In *CVPR*, pages 470–478, 2023. 3
- [71] Honey Gupta and Kaushik Mitra. Toward unaligned guided thermal super-resolution. *TIP*, 31:433–445, 2021. 3
- [72] Priya Kansal and Sabari Nathan. A multi-level supervision model: A novel approach for thermal image super resolution. In *CVPR*, pages 94–95, 2020. 3
- [73] Kaiwen Cai, Qiyue Xia, Peize Li, John Stankovic, and Chris Xiaoxuan Lu. Robust Human Detection under Visual Degradation via Thermal and mmWave Radar Fusion. In *EWSN*, 2023. 3
- [74] Marina Ivašić-Kos, Mate Krišto, and Miran Pobar. Human detection in thermal imaging using YOLO. In *Proceedings of the 2019 5th International Conference on Computer and Technology Applications*, pages 20–24, 2019. 3
- [75] Ali Haider, Furqan Shaukat, and Junaid Mir. Human detection in aerial thermal imaging using a fully convolutional regression network. *Infrared Physics & Technology*, 116:103796, 2021. 3
- [76] Ganbayar Batchuluun, Dat Tien Nguyen, Tuyen Danh Pham, Chanhum Park, and Kang Ryoung Park. Action recognition from thermal videos. *IEEE Access*, 7:103893–103917, 2019. 3
- [77] Meng Ding, Yuanyuan Ding, Li Wei, Yiming Xu, and Yunfeng Cao. Individual Surveillance Around Parked Aircraft at Nighttime: Thermal Infrared Vision-Based Human Action Recognition. *IEEE Transactions on Systems, Man, and Cybernetics: Systems*, 53(2):1084–1094, 2022. 3
- [78] Marcos Lupión, Aurora Polo-Rodríguez, Javier Medina-Quero, Juan F Sanjuan, and Pilar M Ortigosa. 3D Human Pose Estimation from multi-view thermal vision sensors. *Information Fusion*, 104:102154, 2024. 3
- [79] I-Chien Chen, Chang-Jen Wang, Chao-Kai Wen, and Shioh-Jyu Tzou. Multi-person pose estimation using thermal images. *IEEE Access*, 8:174964–174971, 2020. 3
- [80] Javier Smith, Patricio Loncomilla, and Javier Ruiz-Del-Solar. Human Pose Estimation using Thermal Images. *IEEE Access*, 2023. 3
- [81] Zülfiye Kütük and Görkem Algan. Semantic segmentation for thermal images: A comparative survey. In *CVPR*, pages 286–295, 2022. 3
- [82] Yeong-Hyeon Kim, Ukcheol Shin, Jinsun Park, and In So Kweon. MS-UDA: Multi-spectral unsupervised domain adaptation for thermal image semantic segmentation. *RA-L*, 6(4):6497–6504, 2021. 3
- [83] Johan Vertens, Jannik Zürn, and Wolfram Burgard. Heatnet: Bridging the day-night domain gap in semantic segmentation with thermal images. In *IROS*, pages 8461–8468. IEEE, 2020. 3
- [84] Chenglong Li, Wei Xia, Yan Yan, Bin Luo, and Jin Tang. Segmenting objects in day and night: Edge-conditioned CNN for thermal image semantic segmentation. *TNNLS*, 32(7):3069–3082, 2020. 3
- [85] Ukcheol Shin, Jinsun Park, and In So Kweon. Deep Depth Estimation From Thermal Image. In *CVPR*, pages 1043–1053, June 2023. 3
- [86] Yawen Lu and Guoyu Lu. An alternative of lidar in nighttime: Unsupervised depth estimation based on single thermal image. In *WACV*, pages 3833–3843, 2021. 3

- [87] Ukcheol Shin, Kyunghyun Lee, Seokju Lee, and In So Kweon. Self-supervised depth and ego-motion estimation for monocular thermal video using multi-spectral consistency loss. *RA-L*, 7(2):1103–1110, 2021. 3
- [88] Namil Kim, Yukyung Choi, Soonmin Hwang, and In So Kweon. Multispectral transfer network: Unsupervised depth estimation for all-day vision. In *AAAI*, 2018. 3
- [89] Shehryar Khattak, Christos Papachristos, and Kostas Alexis. Keyframe-based thermal–inertial odometry. *Journal of Field Robotics*, 37(4):552–579, 2020. 3
- [90] Saputra, Muhamad Risqi U. and Lu, Chris Xiaoxuan and de Gusmao, Pedro Porto B. and Wang, Bing and Markham, Andrew and Trigoni, Niki. Graph-based thermal–inertial slam with probabilistic neural networks. *TRO*, 38(3):1875–1893, 2022. 3
- [91] Young-Sik Shin and Ayoung Kim. Sparse depth enhanced direct thermal-infrared SLAM beyond the visible spectrum. *RA-L*, 4(3):2918–2925, 2019. 3
- [92] Muhamad Risqi U Saputra, Pedro PB de Gusmao, Chris Xiaoxuan Lu, Yasin Almalioglu, Stefano Rosa, Changhao Chen, Johan Wahlström, Wei Wang, Andrew Markham, and Niki Trigoni. Deeptio: A deep thermal-inertial odometry with visual hallucination. *RA-L*, 5(2):1672–1679, 2020. 3
- [93] Ruoshi Liu and Carl Vondrick. Humans as Light Bulbs: 3D Human Reconstruction from Thermal Reflection. In *CVPR*, pages 12531–12542, 2023. 3
- [94] Agata Sage, Daniel Ledwoń, Jan Juszczak, and Paweł Badura. 3D Thermal Volume Reconstruction from 2D Infrared Images—a Preliminary Study. In *Innovations in Biomedical Engineering*, pages 371–379. Springer, 2021. 3
- [95] Sebastian Schramm, Phil Osterhold, Robert Schmoll, and Andreas Kroll. Combining modern 3D reconstruction and thermal imaging: Generation of large-scale 3D thermograms in real-time. *Quantitative InfraRed Thermography Journal*, 19(5):295–311, 2022. 3
- [96] Teledyne FLIR. *Boson - Uncooled, Longwave Infrared (LWIR) OEM Thermal Camera Module*, 2024. Accessed: 2024-02-13. 4
- [97] Martin A. Fischler and Robert C. Bolles. Random Sample Consensus: A Paradigm for Model Fitting with Applications to Image Analysis and Automated Cartography. *Communications of the ACM*, 24(6):381–395, 1981. 4
- [98] Ignacio Vizzo, Tiziano Guadagnino, Benedikt Mersch, Louis Wiesmann, Jens Behley, and Cyrill Stachniss. Kiss-icp: In defense of point-to-point icp—simple, accurate, and robust registration if done the right way. *RA-L*, 8(2):1029–1036, 2023. 4
- [99] Google LLC. MediaPipe Hands. <https://github.com/google/mediapipe>, 2020. Accessed: 2024-02-13. 5
- [100] Alexander Kirillov, Eric Mintun, Nikhila Ravi, Hanzi Mao, Chloe Rolland, Laura Gustafson, Tete Xiao, Spencer Whitehead, Alexander C Berg, Wan-Yen Lo, et al. Segment anything. *arXiv preprint arXiv:2304.02643*, 2023. 5
- [101] Xizhou Zhu, Weijie Su, Lewei Lu, Bin Li, Xiaogang Wang, and Jifeng Dai. Deformable detr: Deformable transformers for end-to-end object detection. In *ICLR*, 2020. 6
- [102] Ashish Vaswani, Noam Shazeer, Niki Parmar, Jakob Uszkoreit, Llion Jones, Aidan N Gomez, Łukasz Kaiser, and Illia Polosukhin. Attention is all you need. *NIPS*, 30, 2017. 6

Checklist

1. For all authors...
 - (a) Do the main claims made in the abstract and introduction accurately reflect the paper’s contributions and scope? [Yes] We elaborate our contributions as a list in the introduction section and briefly explain them in the abstract.
 - (b) Did you describe the limitations of your work? [Yes] See Sec. 5
 - (c) Did you discuss any potential negative societal impacts of your work? [N/A] There is no societal impact of this work.

- (d) Have you read the ethics review guidelines and ensured that your paper conforms to them? [Yes] We have reviewed the ethics review guidelines and make sure we obey all rules for this research.
2. If you are including theoretical results...
- (a) Did you state the full set of assumptions of all theoretical results? [N/A] This work does not contribute to the theoretical results.
- (b) Did you include complete proofs of all theoretical results? [N/A] This work does not contribute to the theoretical results.
3. If you ran experiments (e.g. for benchmarks)...
- (a) Did you include the code, data, and instructions needed to reproduce the main experimental results (either in the supplemental material or as a URL)? [No] We will release our code upon the acceptance of this paper.
- (b) Did you specify all the training details (e.g., data splits, hyperparameters, how they were chosen)? [Yes] We describe them in our main paper and supplementary document.
- (c) Did you report error bars (e.g., with respect to the random seed after running experiments multiple times)? [No] In line with the state-of-the-art 3D hand pose estimation works, we do not report error bars for our experiment results.
- (d) Did you include the total amount of compute and the type of resources used (e.g., type of GPUs, internal cluster, or cloud provider)? [Yes] We include the type of GPUs in the main paper.
4. If you are using existing assets (e.g., code, data, models) or curating/releasing new assets...
- (a) If your work uses existing assets, did you cite the creators? [Yes] We use the official code of HTT [15] and A2J-transformer [46] to reproduce their results on our dataset, which have been cited.
- (b) Did you mention the license of the assets? [Yes] We mention the license of the official codes of HTT and A2J-Transformer in the supplementary document.
- (c) Did you include any new assets either in the supplemental material or as a URL? [Yes] We include the datasheet and the download URL of our dataset in the supplemental document.
- (d) Did you discuss whether and how consent was obtained from people whose data you're using/curating? [Yes] We claim in the footnote that participant consent forms were signed before the collection.
- (e) Did you discuss whether the data you are using/curating contains personally identifiable information or offensive content? [Yes] We discuss in the supplementary document.
5. If you used crowdsourcing or conducted research with human subjects...
- (a) Did you include the full text of instructions given to participants and screenshots, if applicable? [N/A] We do not give written instructions to our participants.
- (b) Did you describe any potential participant risks, with links to Institutional Review Board (IRB) approvals, if applicable? [N/A] There is no potential participant risks.
- (c) Did you include the estimated hourly wage paid to participants and the total amount spent on participant compensation? [N/A] Our participants are volunteer.